Astron. Astrophys. 357, 587–596 (2000)

ASTRONOMY AND ASTROPHYSICS

Element abundances in cool white dwarfs

I. The DZA white dwarfs L 745-46A and Ross 640⋆

D. Koester⋆⋆ and B. Wolff

Institut für Theoretische Physik und Astrophysik, Universität Kiel, 24098 Kiel, Germany (koester,wolff@astrophysik.uni-kiel.de)

Received 28 January 2000 / Accepted 14 March 2000

Abstract. The standard explanation for the presence of photospheric metals in white dwarfs of spectral type DZ and related types is a combination of episodic accretion from the interstellar medium and diffusion of heavy elements downwards in the atmosphere on time scales of typically 10^6 years. Much of the empirical data on atmospheric parameters and element abundances available in the literature is based on International Ultraviolet Explorer spectra with low signal-to-noise and on atmospheric modeling, which does not include recent advances in input physics. We have therefore decided to address this problem again, using modern UV observations of the Hubble Space Telescope (HST), if available, and a new generation of theoretical models. In this paper we start with an analysis of the DZA white dwarfs L 745-46A and Ross 640. These are key objects since they contain both hydrogen and metals in their atmospheres. Excellent UV spectra obtained with the Faint Object Spectrograph (FOS) onboard HST make them good test cases for the methods to be applied in future work on other objects and for the accuracy, which can be achieved. We have determined the atmospheric parameters $T_{\rm eff}$ and $\log g$ as well as hydrogen abundances and abundances of several heavy elements. The results are in good agreement with the theoretical predictions of Dupuis and collaborators. Particular emphasis is placed on a discussion of the remaining problems in the input physics and the corresponding uncertainties of the final results.

Key words: stars: abundances – stars: atmospheres – stars: white dwarfs – ultraviolet: stars

1. Introduction

White dwarf atmospheres are usually dominated by either hydrogen or helium. The main reason for this mono-elemental composition is the high surface gravity resulting in a separation of the elements according to their weight (Schatzman 1949, 1958).

At the cool end of the white dwarf sequence ($T_{\rm eff} \lesssim 15\,000$ K) traces of elements heavier than helium are found in several mostly helium-rich objects (spectral types DZ and DBZ). These elements cannot be of primordial origin since the diffusion time scales for element separation are much shorter than the cooling times for white dwarfs from the end of the asymptotic giant branch down to these low temperatures. Selective radiation pressure, which is able to compete against gravity at $T_{\rm eff} \gtrsim 50\,000$ K (e.g. Vauclair et al. 1979, Chayer et al. 1995, Wolff et al. 1998), is ineffective at lower temperatures so that other mechanisms have to be considered.

In the case of carbon in DQ white dwarfs – not discussed in this paper – convective dredge-up is the most probable process (Koester et al. 1982, Pelletier et al. 1986). An explanation for the presence of other metals in white dwarfs of spectral types DZ and DBZ is provided by the assumption of accretion from the interstellar medium. Dupuis et al. (1992, 1993a, b) have put this idea on a sound theoretical basis and have compared in detail their predictions with available observations. The *two-phase accretion model* assumes that accretion onto white dwarfs is small (typically $10^{-20}\,M_\odot\,{\rm yr}^{-1}$) most of the time but is much larger ($\approx\ 5\cdot10^{-15}\,M_\odot\,{\rm yr}^{-1}$) during rare and short passages through dense interstellar clouds. Heavy elements are expected to become visible only during and shortly after such cloud encounters. They disappear exponentially on the "diffusion timescale" of typically a million years. Since these timescales are different for different elements the individual abundances and the abundance ratios of the metals vary in a characteristic way with time after the encounter, if e.g. solar abundances are assumed for the accreted material. Dupuis et al. (1993b) have demonstrated that the observed levels of metals as well as their ratios can be accounted for by this model – at least within the large observational uncertainties.

In spite of this success of the two-phase accretion model there are several remaining problems. The most notable is related to the hydrogen abundance in helium-rich white dwarfs. As the lightest element, hydrogen is not subject to downward diffusion and should be accumulated in the upper layers of the atmosphere. However, hydrogen is rarely observed in these ob-

Send offprint requests to: B. Wolff

⋆ Based on observations made with the NASA/ESA Hubble Space Telescope, obtained at the Space Telescope Science Institute, which is operated by the Association of Universities for Research in Astronomy, Inc., under NASA contract NAS 5-26555. These observations are associated with proposal ID 6450. Based on observations collected at the European Southern Observatory, Chile (ESO No. 54.D-0402)

⋆⋆ Visiting Astronomer, German-Spanish Astronomical Centre, Calar Alto, operated by the Max-Planck-Institute for Astronomy, Heidelberg, jointly with the Spanish National Commission for Astronomy

jects so that it seems that the accretion of hydrogen is prevented, i. e. the composition of the acccreted matter does not have solar hydrogen/metal ratios. This led to the assumption of mechanisms screening hydrogen (e.g. "propeller mechanism", Wesemael & Truran 1982). Another possible solution has recently been proposed by Bergeron et al. (1997) in their study of very cool white dwarfs: Because of the high pressures in pure helium atmospheres, the relevant atomic hydrogen levels do not exist and hydrogen accreted onto helium-rich white dwarfs would remain invisible. In the objects considered in this study the pressure is much lower than in the pure He atmospheres considered by these authors, and we do not believe that this mechanism can simultaneously explain the observed underabundance of hydrogen and the presence of metals.

On the other hand, hydrogen *is* present in some He-rich white dwarfs at somewhat higher temperatures (the DBA stars at $T_{\rm eff} \geq 14\,000$ K) and can only be explained by accretion (MacDonald & Vennes 1991). Why hydrogen is sometimes accreted, and sometimes not, or at which temperatures hydrogen accretion is inhibited, is currently an unsolved problem, which can best be studied in white dwarfs showing simultaneously both hydrogen *and* metals.

Much of the observational data used by Dupuis et al. (1992, 1993a, b) is based on IUE (International Ultraviolet Explorer) spectra, and a significant fraction of the analyses has been performed by our group in Kiel 10 to 20 years ago. It is well known that the S/N obtained with that small telescope for faint white dwarfs is rather low, and the abundance determinations have large uncertainties, or are only upper limits in many cases. This situation has improved with the advent of the Hubble Space Telescope (HST), which allowed for the first time to obtain high S/N spectra of the UV region from 1150 to 3000 Å for a number of interesting objects. In addition, a completely new reduction of all IUE spectra is now available in the final archive, which has also improved the S/N compared to the original data.

During the same period there have also been advances on the theoretical side in the art of computing model atmospheres as well as in the input data. NLTE effects are in general negligible at these low temperatures. However, the densities and pressures are high, and therefore non-ideal effects in the equation of state (EOS) may become significant. A major progress has been the development of the Hummer-Mihalas occupation probability mechanism and the corresponding effects on occupation numbers (and therefore line strengths), dissolution of bound states near the series limits, and increased ionization over the ionization given by purely thermal effects as described by the Saha equation. This latter effect is often called pressure ionization, although usually the ionization fraction is extremely small and real pressure ionization is not reached within the atmospheres. Other changes to the input physics compared to previous generations of our atmosphere codes are mentioned in the next section.

Some tests with our more recent models using old IUE spectra have shown that the results can significantly change. Moreover, the new data, especially from HST observations, allow abundance determinations for elements, which could not even be identified in the IUE spectra, thus providing much more stringent constraints on the theoretical scenario. We have therefore concluded that it is worthwhile to address this area again, with the ultimate goal of providing an accurate and consistent set of empirical abundance determinations, which can then be compared with theory.

In a recent study we have analyzed HST, IUE, and optical spectra of GD 40 and a very similar object (HS 2253+8023), discovered in follow-up spectroscopy of quasar candidates from the Hamburg Quasar Survey (Friedrich et al. 1999). GD 40 is the prototype of the class of DBZ objects, which are still hot enough to show He I lines in optical spectra. In this study we turn to two objects in the range below 10 000 K, where a pure He atmosphere produces only a continuous spectrum, defining the spectral type DC, if no metals – and therefore no spectral lines – are present. L 745-46A and Ross 640 are well known representatives of the spectral type DZA, which means that they show metal traces (e.g. Ca II) and faint Balmer lines (in most cases Hα only), which makes them especially interesting in view of the hydrogen problem discussed above. Both objects have been observed with HST/FOS (see below). These are among the best observations available for any white dwarf with metal traces. We will use them to establish and test our analysis methods, and to determine the remaining uncertainties due to difficult input physics. The results will be used for future work with the same theoretical models, but for other objects and spectral types, where the observations are unfortunately of lower quality.

2. Model atmospheres and input physics

The general procedures used for the calculation of theoretical atmosphere models and synthetic spectra have been described in some detail by Finley et al. (1997). The most important changes compared to the input physics used e.g. by Koester et al. (1982) or Zeidler-K.T. et al. (1986) are

- use of the Hummer-Mihalas-Däppen occupation probability formalism as described in Hummer & Mihalas (1988), Mihalas et al. (1988), Däppen et al. (1988), and Mihalas et al. (1990). We use small modifications for the critical field strength and the neutral radii as suggested by Bergeron et al. (1991) and Bergeron (1993)
- Pressure ionization is treated exactly as in Mihalas et al. (1988); specifically, we use their values for the "free" parameters
- inclusion of H_2^+ and He_2^+ photodissociation and free-free absorption coefficients after Stancil (1994)
- use of new hydrogen Stark broadening tables for many Lyman, Balmer, and Paschen lines calculated by Lemke (1997) using the theory and codes of Vidal et al. (1973)
- improved calculation of Lα broadening by charged and neutral perturbers according to the work of Allard and collaborators (Allard & Kielkopf 1991, Allard & Koester 1992, Allard et al. 1994, 1998)
- new Stark broadening tables for HeI lines, calculated and provided by Beauchamp et al. (1997, priv. comm.)

2.1. Equation of state and ionization fraction

Atmospheres for very cool white dwarfs with zero metallicity have been studied in great detail by Bergeron et al. (1995). Their prefered EOS is a modified version of the EOS of Saumon & Chabrier (1994) and Saumon et al. (1995). This model predicts much lower ionization, and pressure ionization at much higher pressures, than earlier work (e.g. Fontaine et al. 1977), a result supported by experimental evidence (Nellis et al. 1984). Even for effective temperatures as low as 4500 K, the electron density given by this model is close to the ideal gas model (using only the unmodified Saha equation) up to pressures of 10^{12} dynes/cm^2. In our present study we consider only much hotter objects, and moreover, the atmospheres are not pure helium but contain traces of elements with much lower ionization potentials. As a consequence the atmospheric pressures are much lower and never exceed 10^{11} dynes/cm^2 even at the bottom of our models at Rosseland optical depths ≥ 1000. Following the discussion and the results of Bergeron et al. (1995) non-ideal effects should be very small.

We use in our standard models (see above) a version of the Hummer-Mihalas EOS which predicts larger non-ideal effects and larger ionization than the Saumon-Chabrier EOS. To test the sensitivity of our results to this uncertainty of the input physics, we have adopted the following procedure: For the analysis we use our standard models; we then repeat the analysis with models, where all non-ideal effects are switched off and the ionization fraction is only determined by thermal effects using the unmodified Saha equation. For the objects of this study at effective temperatures of about 8000 K both calculations give exactly the same results, i. e. the emergent flux differs by less than 0.2% if models calculated with and without non-ideal effects are compared. This demonstrates that these effects are indeed negligible.

2.2. Lyman α wing

The presence of photospheric hydrogen in L 745-46A and Ross 640 has been discovered through the observation of Balmer lines by Koester (1987) and Liebert (1977), respectively. It has to be expected, therefore, that Lα as the resonance line originating from the ground state is also very strong, and indeed it was obvious from the first test calculations of the UV spectrum that the predicted UV flux is much too high, if Lα is not included. However, model calculations of this line using the classical van-der-Waals broadening by neutral helium result in a Lα wing extending far into the optical region, which is not observed. The same is true for profiles calculated with the quasi-molecular broadening theory by Allard (priv. comm.).

In order to be able to analyze the metal lines on the wing of Lα between 2000 and 3000 Å, Koester & Allard (1995) have weakened the line wing by an exponential function so that the shape of the observed spectrum can be roughly reproduced. Since this artificial procedure is rather unsatisfactory, we have for this study made a new attempt to obtain a more realistic physical description. This is based on the realization that the failure of the quasi-molecular calculation, which has been so successful in DA white dwarfs, is due to the neglect of two effects in the first calculations by Allard (priv. comm.): the variation of the transition probability with the distance between emitter and perturber and the effect of the strongly repulsive potential between H and He atoms at close distances, which are important for the far line wings.

Since we are only interested in the very far wings (the line center, even out to 1500 Å or more, is completely saturated in the spectra), we have used the quasistatic limit of the theory for the multiperturber autocorrelation function $g(s)$ as given by Eq. (59) in the review by Allard & Kielkopf (1982):

$$g(s) = 4\pi \int_0^\infty R^2\, dR[1 - \exp(-i\Delta V(R)\, s/\hbar)] \; .$$

The integration is over the distance R between emitter and perturber, implicitely assuming that the perturber density is homogenous (not influenced by the interaction with the emitter) and that the transition probability for the transition considered is also independent of R and equal to the transition probability at large distances; $\Delta V(R)$ is the difference potential between upper and lower state of the transition, which is a function of perturber distance. In this simple picture it is rather obvious, how this equation has to be modified to be more physically realistic, if very high particle densities and close collisions are important:

$$g(s) \; = \; 4\pi \int_0^\infty p(R)\, \exp(-V(R)/kT)]R^2\, dR \\ [1 - \exp(-i\Delta V(R)\, s/\hbar)],$$

where $p(R)$ is the transition probability and $V(R)$ the interaction energy between emitter in the lower state (considering Lα absorption) and the perturber. The Boltzmann factor here takes into account that in thermal equilibrium the density of perturbers very close to the H atom will be lower because of the strongly repulsive potential. Molecular potential curves and transition probabilities for the H–He system were obtained from Theodorakopoulos et al. (1987). The line profile is finally obtained in the usual way through the Fourier transform of the autocorrelation function (see Allard & Kielkopf 1982).

Somewhat to our surprise, this extremely simple procedure results in theoretical line profiles in our models, which agree very well with the observed flux distribution in both objects studied, at the same hydrogen abundances that are infered from the analysis of Hα (or Hβ). Fig. 1 shows the new Lα wing and a comparison with the observation of L 745-46A. Since the shape of the observed line and the overall ultraviolet and optical flux distribution (see Sects. 4 and 5) are reproduced very well, we are quite confident that this is a realistic description of the Lα profiles under the extreme conditions of our cool atmospheres, where perturber densities may be as high as 10^{21} cm^{-3}.

3. Observations

L 745-46A has been observed with the Faint Object Spectrograph (FOS) of HST in Cycle 1. Shipman et al. (1995) have

Table 1. Observations

WD Number	Name	Instrument	Date	Time / sec	λ/ Å	$\Delta\lambda$/Å
0738−172	L 745-46A	HST/FOS, G160L	92/06/15	4800	1150–2500	6.9
		HST/FOS, G270H	92/06/15	1200	2225–3300	2.1
		ESO, 3.6m, EFOSC	95/02/03		3720–6820	15.5
1626+368	Ross 640	HST/FOS, G160L	96/07/06	900	1150–2500	6.9
		HST/FOS, G270H	96/07/06	3700	2225–3300	2.1
		Calar Alto	95/09/19	3600	3730–5075	4.0

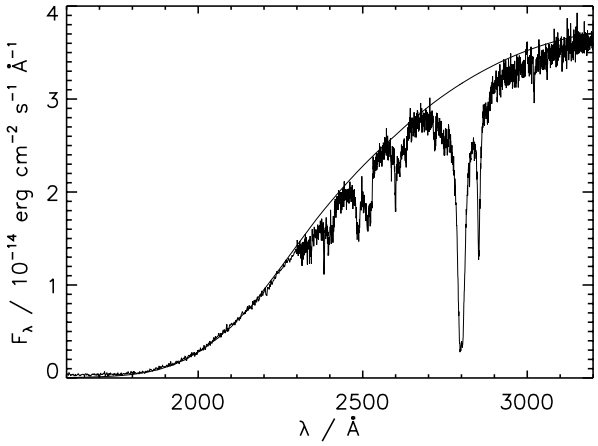

Fig. 1. L 745-46A: Lα line. The metal lines are described in Fig. 5

presented the spectra and have identified several features. In addition, we also use a low resolution optical spectrum obtained at ESO/La Silla showing Hα and the H and K lines of Ca II, and a photometric optical scan from Stone & Baldwin (1983). Koester & Allard (1995, 1996) have already analyzed these observations. In this paper, we continue their investigation.

For Ross 640 we use own observations with FOS obtained in Cycle 6 together with an optical spectrum taken at the Calar Alto observatory and the optical scan from Oke (1974). Table 1 contains an overview of the observations.

4. L 745-46A

4.1. Effective temperature and hydrogen abundance

The effective temperature of L 745-46A can be determined from the optical and ultraviolet flux distribution. As a first step, we have calculated model atmospheres with $\log g = 8.0$ and have fitted the model flux to the optical scan near 7000 Å to account for the solid angle. Since the strong Lα line dominates the flux in the ultraviolet and is also important at optical wavelengths through the blanketing effect the hydrogen abundance has to be determined simultaneously with $T_{\rm eff}$. This abundance is derived from Hα. A visual comparison shows that the flux distribution and Hα can both be reproduced with $T_{\rm eff} = 7500$ K and $\log {\rm He/H} = -3.1$.

Fig. 2 shows the measured flux distribution together with model calculations for $T_{\rm eff} = 7300$, 7500, and 7700 K. Our model for 7500 K can reproduce the overall distribution although the synthetic flux seems to be systematically too high at $\lambda > 5000$ K. The fit in this region could be improved with a different scaling of the model but then the blue part of the optical scan could only be reproduced with higher temperatures. Since these are incompatible with the ultraviolet we have chosen 7500 K as a compromise. The models for 7300 K and 7700 K include most observed values in the blue and ultraviolet so that we finally adopt $T_{\rm eff} = 7500 \pm 200$ K. The error should be a good representation of the remaining uncertainties of the fit.

The solid angle determined from the the model with $T_{\rm eff} = 7500$ K and the optical scan can be used to calculate the gravity. This is possible because the model flux depends only weakly on $\log g$. Together with the parallax of Liebert et al. (1988) and the mass-radius relation of Wood (1994, "thick" hydrogen layers) we determine a gravity of $\log g = 8.07 \pm 0.18$. This justifies the previously assumed value. The uncertainties reflect the uncertainties in $T_{\rm eff}$ and parallax. For the remaining calculations we assume $\log g = 8.0 \pm 0.25$.

In Fig. 3 we show the Hα line together with the best fit for $\log {\rm H/He} = -3.1$ and $T_{\rm eff} = 7500$ K. Additional models with $\log {\rm H/He} = -3.15$ and -3.05 are also plotted for comparison. Taking into account the uncertainties in $T_{\rm eff}$ and $\log g$, the best solution is $\log {\rm H/He} = -3.10 \pm 0.35$ (± 0.4, if uncertainties of the electron density are also considered, see below). Within these limits, the general shape of the model spectrum and thus the determination of $T_{\rm eff}$ are independent of the hydrogen abundance.

4.2. Metal abundances

The optical spectrum contains in addition to Hα also the H and K lines of Ca II (Fig. 4). Further metals can be detected in ultraviolet spectra. The FOS observations show lines of Mg I, Mg II, Si I, Fe I, and Fe II. We cannot confirm the presence of C I (1930 Å) – reported by Zeidler-K.T. et al. (1986) – or other carbon lines, a conclusion also reached by Shipman et al. (1995). Fig. 5 shows a part of the FOS spectrum with the relevant features together with a model fit. The element abundances for $T_{\rm eff} = 7500$ K and $\log g = 8.0$ are given in Table 2. As for the determination of $T_{\rm eff}$ and He/H we have not used a formal fit procedure since the the uncertainties in the input physics and in $T_{\rm eff}$ and $\log g$ are the most dominant error sources. In the following, we discuss the fits of individual elements and estimate uncertainties of the abundances.

The most severe problems arise for iron. As can be seen from Fig. 5 our model fails to reproduce the Fe I lines or – in other

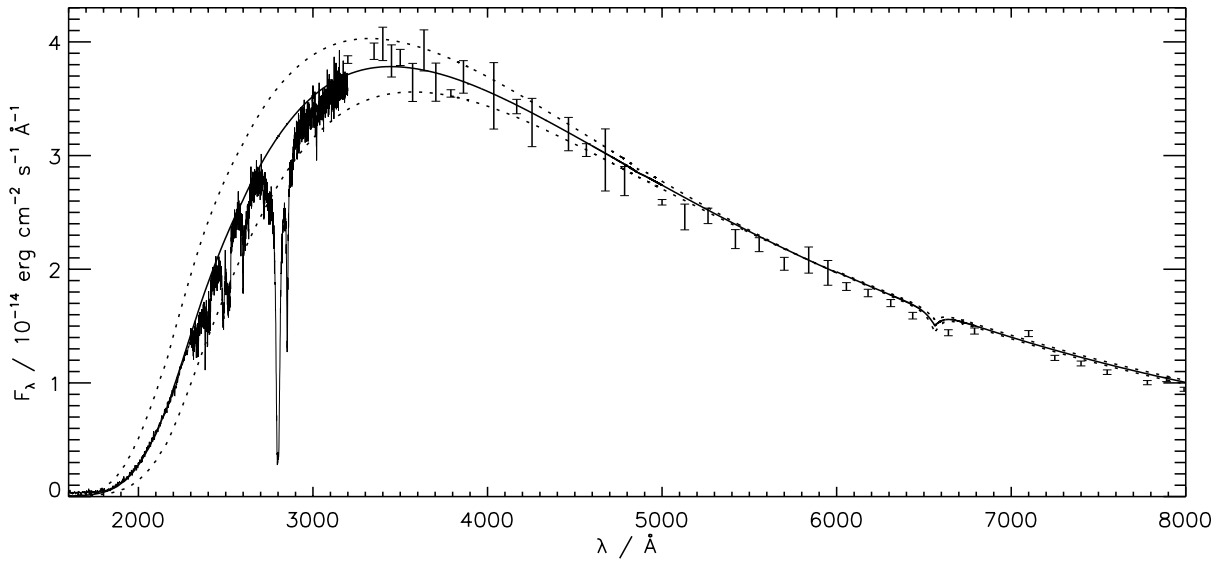

Fig. 2. Flux distribution of L 745-46A: Optical scan and FOS spectrum together with models for $T_{\rm eff} = 7300$, 7500, and 7700 K. The used hydrogen abundance is $\log {\rm H/He} = -3.1$

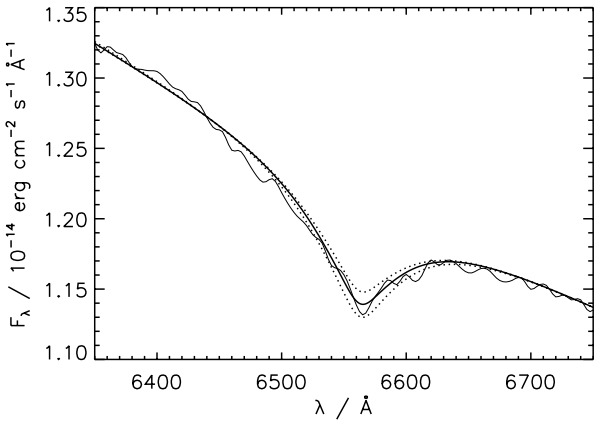

Fig. 3. L 745-46A: Fit to the Hα line with $T_{\rm eff} = 7500$ K and $\log {\rm H/He} = -3.15, -3.1, -3.05$

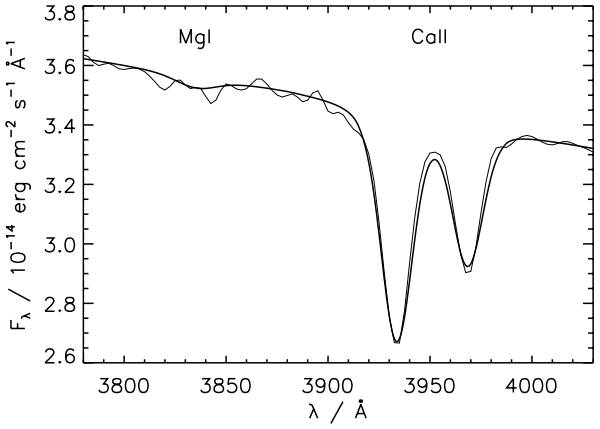

Fig. 4. L 745-46A: Fit to the Ca II lines with $T_{\rm eff} = 7500$ K and $\log {\rm Ca/He} = -10.60$. The Mg I lines are compatible with the Mg abundance of $\log {\rm Mg/He} = -9.05$ as derived from the ultraviolet lines

words – the relative strengths of Fe I compared to Fe II. Whereas most Fe II lines can be reproduced very nicely with $\log {\rm Fe/He} = -9.8$ all Fe I lines are too weak. It is not possible to achieve a reasonable fit by increasing the iron abundance: The Fe I lines would require $\log {\rm Fe/He} = -9.2$ which is incompatible with Fe II.

There are two possible explanations for this discrepancy. The first assumption is that the number of Fe I lines considered in the model calculations could be too low. However, increasing the number of Fe I lines between 2450 Å and 2500 Å from 27 as in Fig. 5 to 1700 does not have any visible effects on the model spectrum. We have also searched the VALD atomic data base (Kupka et al. 1999) for additional lines and have compared oscillator strengths with our values from the Kurucz lists (Kurucz 1991) but we did not find significant differences.

The second possibility is that the ionization balance between Fe I and Fe II is not calculated correctly in the model. As discussed in Sect. 2.1, the interactions of charged and neutral particles are taken into account according to the Hummer-Mihalas-Däppen EOS (Mihalas et al. 1990). Since this procedure tends to overestimate the degree of ionization (Bergeron et al. 1995) we have also calculated ionization with the Saha equation only – without considering any non-ideal effects. Since this only affects the atmospheric structure in the deepest layers of our models and not the model spectrum non-ideal effects seem to be rather unimportant for the analysis of L 745-46A.

In general, higher Fe I/Fe II ratios can be obtained by lowering the effective temperature or increasing the number of free electrons. Changes of the temperature can be ruled out: For a consistent fit of both the Fe I and Fe II lines $T_{\rm eff}$ has to be decreased to ≈ 6000 K. This value is, of course, incompatible with the optical scan. Therefore, an increase of the electron density seems to be more appropriate.

Table 2. Results of the model atmosphere analysis and comparison with previous results

Object	$T_{\rm eff}$/K	$\log g$	$\log {\rm H/He}$	Reference
L 745-46A	7500 ± 200	8.0 ± 0.2	-3.1 ± 0.4	this paper
	7800			Zeidler86
			-3.2	Koester96
Ross 640	8500 ± 200	8.0 ± 0.15	-3.3 ± 0.3	this paper
	8800		-3.5	Zeidler86
	8800		-3.1	Liebert87

Object	$\log {\rm C/He}$	$\log {\rm Mg/He}$	$\log {\rm Al/He}$	$\log {\rm Si/He}$	$\log {\rm Ca/He}$	$\log {\rm Fe/He}$	Reference
L 745-46A	< -8.0	-9.05 ± 0.20	< -9.0	-9.4 ± 0.35	-10.60 ± 0.20	-9.8 ± 0.20	this paper
	-7.1	-9.0		-9.5	-10.4	< -11.0	Zeidler86
		-9.3		< -9.4	-10.7	-9.8	Koester96
Ross 640	< -9.0	-7.25 ± 0.65	< -8.25	-7.5 ± 0.5	-8.65 ± 0.45	-8.3 ± 0.15	this paper
	-6.0	-7.15		-7.3	-9.1	-8.3	Zeidler86
		-6.7			-9.1	-8.7	Liebert87

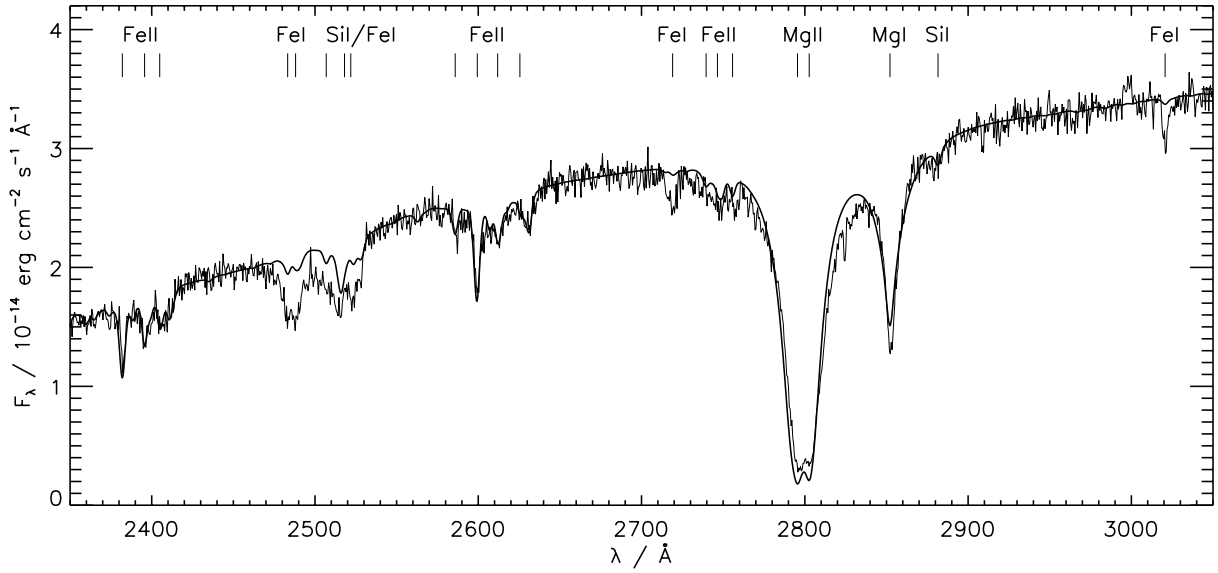

Fig. 5. L 745-46A: Part of the FOS spectrum together with the best model fit. The most prominent lines are identified

Free electrons are provided mostly through the ionization of hydrogen. The abundances of metals are too low so that they do not contribute significantly to the electron density, although their ionization potentials are much lower than that of hydrogen. It is unlikely that hydrogen is more ionized than calculated by our models (see above). However, it may be possible that metals which could not be detected spectroscopically contribute significantly to the electron number.

For a general test of the influence of higher electron densities we have artificially increased the abundances of hydrogen or magnesium for the calculation of the EOS, but have left the abundances unchanged for the determination of the synthetic spectrum. This allows us to increase the number of free electrons without changing spectral lines directly. The two elements were chosen as examples because of their different ionization potentials (7.6 eV for magnesium and 13.6 eV for hydrogen) so that the electron density is changed in different depths.

The Fe I and Fe II lines can be reproduced simultaneously if the (EOS) abundances are increased to $\log {\rm Mg/He} = -6.8$ or $\log {\rm H/He} = -1.0$ and $T_{\rm eff}$ is adjusted to 7300 K or 7800 K, respectively. However, the higher electron density changes also the ionization balance of magnesium so that Mg I and Mg II lines cannot be reproduced simultaneously any more.

Changing the electron density in different depths has different side-effects. The increase of the magnesium abundance increases the electron density mainly in the outer atmospheric regions. This does not change the atmospheric structure significantly so that the flux distribution can still be reproduced. However, the higher hydrogen abundance mainly affects deeper layers with the result that the overall flux distribution and the shape of the Hα line are changed significantly.

A fit of the metal lines using atmospheres with higher electron densities requires also adjusted abundances. If magnesium is used as the electron donator then the logarithmic abundances

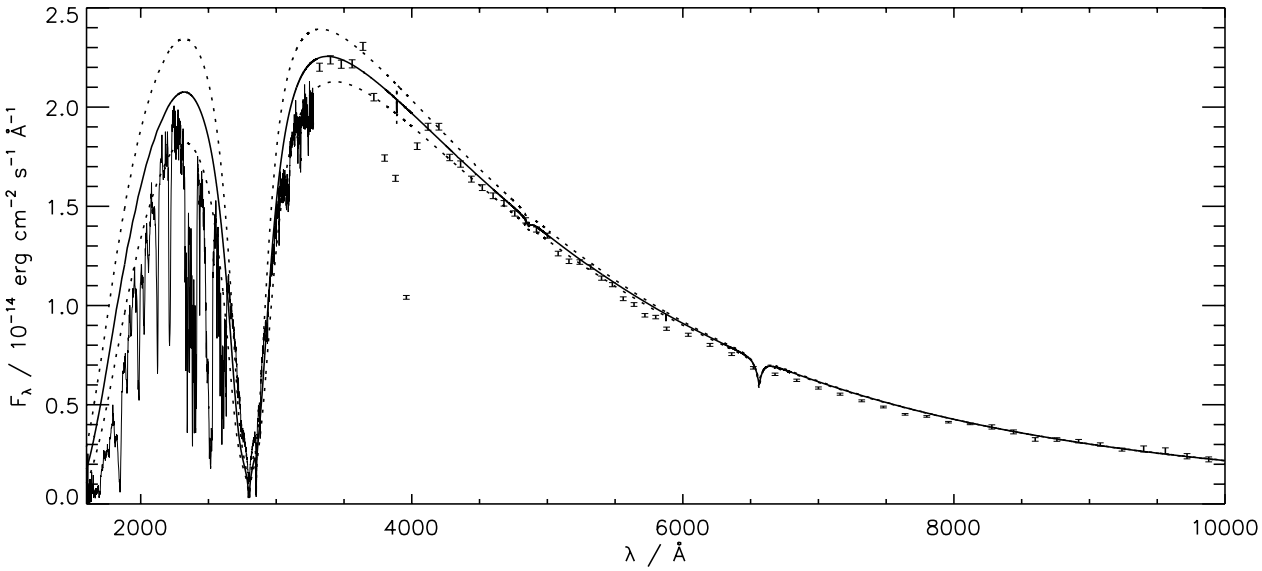

Fig. 6. Flux distribution of Ross 640: Optical scan and FOS spectrum together with models for $T_{\rm eff} = 8300$, 8500, and 8700 K. The used hydrogen and magnesium abundances are $\log {\rm H/He} = -3.3$ and $\log {\rm Me/He} = -7.25$, respectively

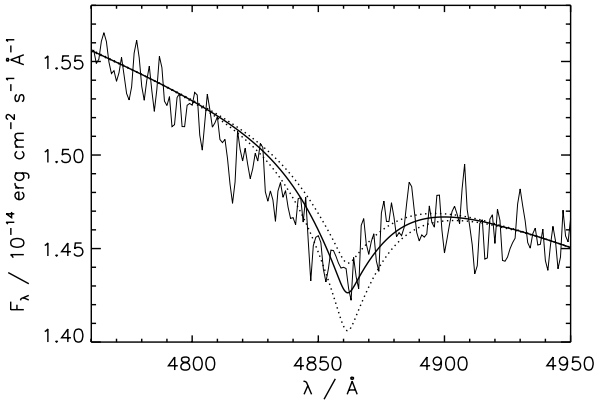

Fig. 7. Ross 640: Fit to the Hβ line with $T_{\rm eff} = 8500$ K and $\log {\rm H/He} = -3.4, -3.3, -3.2$

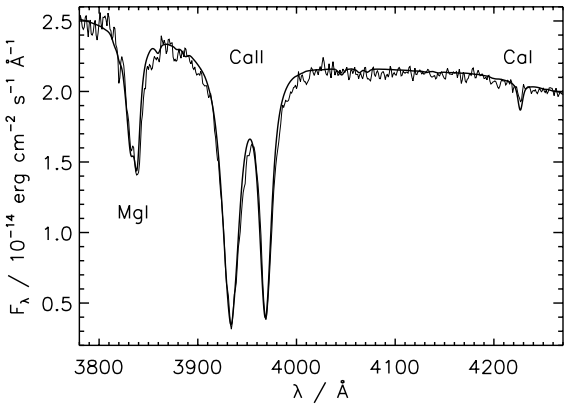

Fig. 8. Ross 640: Fit to the Mg I, Ca I and Ca II lines with $T_{\rm eff} = 8500$ K, $\log {\rm Mg/He} = -7.25$, and $\log {\rm Ca/He} = -8.65$

are changed by about 0.1 to 0.2. For hydrogen, the abundances need to be changed by about a factor of 10.

Since the ionization balance of magnesium is severely affected by an increase of the electron density we do not believe that this is the final solution for the problem with Fe I. Therefore, we adopt the original abundances obtained without changing the number of free electrons and regard the electron density as an additional uncertainty for the metal abundances. These uncertainties are added (quadratically) to the uncertainties arising from $T_{\rm eff}$ and $\log g$. Table 2 lists the abundances together with the uncertainties. We consider only magnesium as electron donator since hydrogen changes also the flux distribution and Hα.

We end this section with some remarks on other elements. The magnesium abundance of $\log {\rm Mg/He} = -9.05$ can reproduce the equivalent widths of the Mg I and Mg II lines but the form of these lines cannot be reproduced in detail. The abundance is in agreement with the optical Mg I lines near 3840 Å which cannot be clearly detected (see Fig. 4). We adopt an additional error of ± 0.1 to account for the uncertainties due to the line shape.

The silicon abundance is based on the Si I line at 2881.6 Å. The lines near 2500 Å are blended by Fe I so that they cannot be used for a reliable abundance determination. Other silicon lines are not visible – in agreement with the value of $\log {\rm Si/He} = -9.4$.

5. Ross 640

5.1. Effective temperature and hydrogen abundance

Effective temperature, gravity, and hydrogen abundance are determined with a procedure similar to the analysis of L 745-46A. The only differences are that we use Hβ instead of Hα to derive the hydrogen abundance and that the strong ultraviolet magnesium lines have to be considered for the model calculations (see Sect. 5.2).

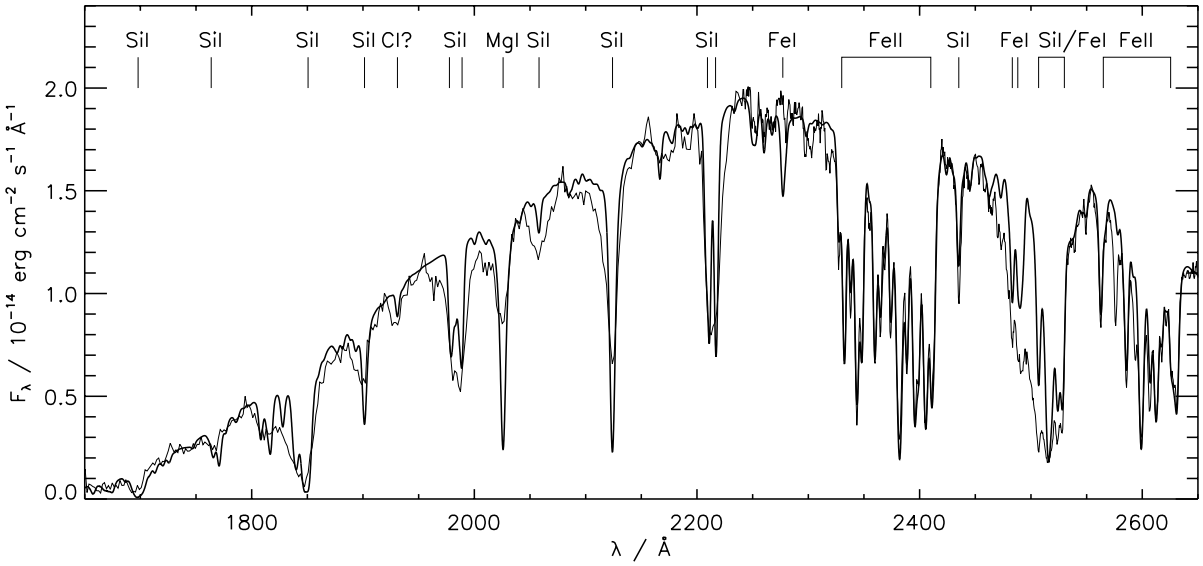

Fig. 9. Ross 640: Part of the FOS spectrum together with the best model fit. The most prominent lines are identified

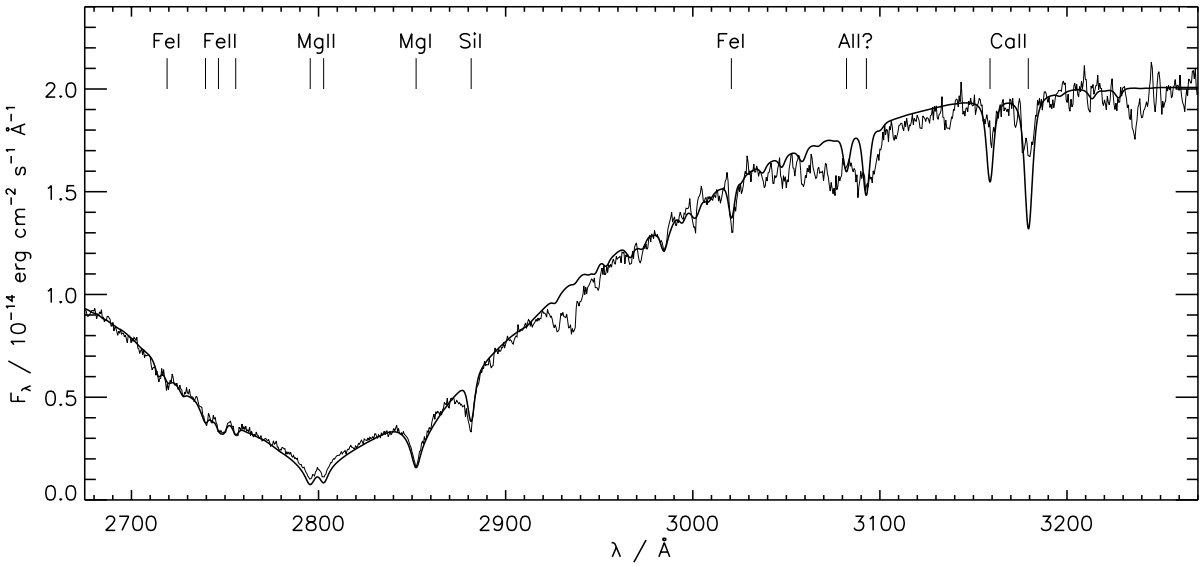

Fig. 10. Ross 640: Part of the FOS spectrum together with the best model fit. The most prominent lines are identified

The flux distribution and Hβ can be reproduced simultaneously with $T_{\rm eff} = 8500 \pm 200$ K (Fig. 6) and $\log {\rm H/He} = -3.3$ (Fig. 7). As in the case of L 745-46A, the error in $T_{\rm eff}$ should be a good representation of the uncertainties of the fit. The solid angle together with the mean parallax from Dahn et al. (1987) and van Altena (1998) and the mass-radius relation of Wood (1994, "thick" hydrogen layers) gives $\log g = 8.0 \pm 0.15$. The uncertainties in $T_{\rm eff}$ and $\log g$ translate in an error of ± 0.3 for the hydrogen abundance.

5.2. Metal abundances

The optical spectrum shows lines of Mg I, Ca I, and Ca II and the FOS spectra lines of Mg I, Mg II, Si I, Ca II, Fe I, Fe II, and probably of C I and Al I. The spectra are presented in Figs. 8, 9, and 10. The element abundances for $T_{\rm eff} = 8500$ K and $\log g = 8.0$ are listed in Table 2. The errors arise from the uncertainties in $T_{\rm eff}$ and $\log g$ and from additional uncertainties in the model fits. These uncertainties are discussed in the following.

The magnesium abundance is derived from the optical Mg I lines near 3840 Å (see Fig. 8) because the width of the ultraviolet lines of Mg II at 2795.5 Å and 2802.7 Å cannot be reproduced. This is demonstrated in Fig. 11 where a model spectrum with these lines is compared to the observation. A better fit can be obtained if the van-der-Waals broadening constant is increased by a factor of ten (from $\log \gamma_6 = 8.140$ to 9.140 for a perturber density of 10^{16} cm^{-3}). However, this can only be regarded as a crude approximation. We use the latter value for the calculation of model atmospheres and spectra in order to approximate the absorption by the ultraviolet Mg II lines.

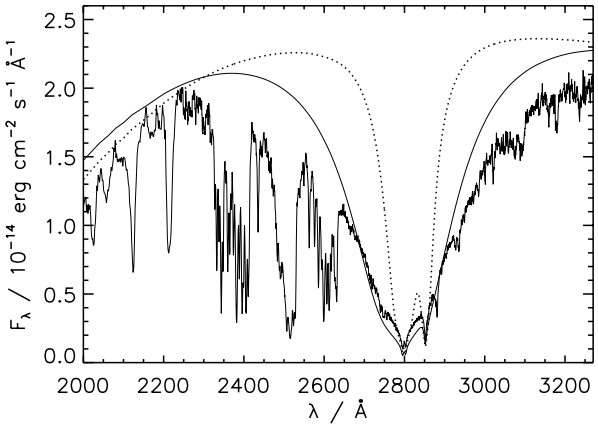

Fig. 11. Ross 640: Ultraviolet Mg I and Mg II lines. Dotted line: Mg II with $\log\gamma_6 = 8.140$. Solid line: Mg II with $\log\gamma_6 = 9.140$. Both models are fitted to the optical scan near 8000 Å

Another problem with magnesium arises from the Mg I line at 2025.8 Å which is too strong in the model with $\log \mathrm{Mg/He} = -7.25$. This line can be reproduced better with $\log \mathrm{Mg/He} = -7.9$.

We have a similar problem with the optical and ultraviolet lines of calcium. The abundance of $\log \mathrm{Ca/He} = -8.65$ given in Table 2 is a compromise between the Ca II lines at 3933.7 Å/3968.5 Å and the Ca I line at 4226.7 Å. These lines could be reproduced better with $\log \mathrm{Ca/He} = -8.75$ or $\log \mathrm{Ca/He} = -8.60$, respectively, whereas the ultraviolet Ca II lines at 3158.7 Å/3179.3 Å require $\log \mathrm{Ca/He} = -9.05$.

The silicon abundance is also a compromise between different lines since some lines are too strong whereas others are too weak. The abundances for carbon and aluminum should be regarded as upper limits.

The iron lines have the same problems as in L 745-46A: From Fe II we derive $\log \mathrm{Fe/He} = -8.3$ but Fe I cannot be reproduced with this abundance. For a simultaneous fit to both ionization stages $T_{\rm eff}$ had to be reduced to ≈ 7750 K. Similar to L 745-46A it is also possible to increase the EOS abundance of magnesium to $\log \mathrm{Mg/He} = -5.5$ resulting in a higher electron density. Again, this cannot be regarded as the final solution since a higher electron density changes also the ionization balance of calcium so that the optical Ca I and Ca II lines cannot be simultaneously reproduced any more. Indeed, for these lines a lower electron density would be more appropriate since Ca I is somewhat too strong compared to Ca II. The uncertainties due to the uncertain electron density are included in the errors listed in Table 2.

6. Discussion

We have determined new element abundances for L 745-46A and Ross 640 and have discussed the uncertainties due to difficult input physics. In Table 2 we compare our results with previous abundance determinations from the literature. The analyses of Zeidler-K.T. et al. (1986) and Liebert et al. (1987) are based on IUE and optical spectra whereas Koester & Allard (1996) could use HST data for L 745-46A.

Our results are in general very similar to previous determinations. The remarkable deviations arise for carbon. We cannot confirm the detection of C I by Zeidler-K.T. et al. Instead, the HST spectra allow to give stringent upper limits for the carbon abundance. A similar improvement can be achieved for iron in L 745-46A: Zeidler-K.T. et al. could only give an upper limit whereas we can now clearly identify iron lines. This demonstrates the progress for faint ultraviolet lines made with HST compared to IUE. Not surprisingly, the HST analysis of Koester & Allard is similar to ours.

All metal abundances in L 745-46A and Ross 640 are in the range of predicted values for accretion from the interstellar medium (Dupuis et al. 1993b). The metal-to-metal abundance ratios are also compatible with the accretion model. The ratios for L 745-46A are now in far better agreement then in previous studies. This is mainly due to the more accurate iron abundance. The disagreement of the Fe/Ca ratio led Dupuis et al. to the assumption that calcium was a factor of eight overabundant in the accreted material if compared to solar abundances. This is not necessary any more.

The hydrogen abundances in L 745-46A and Ross 640 are amoung the highest observed in cool helium-rich white dwarfs. From Fig. 8 and Eq. (4) in the paper of Dupuis et al. (1993b) we estimate that an average accretion rate of $\approx 2 \cdot 10^{-19} M_\odot\,\mathrm{yr}^{-1}$ is necessary to provide these abundances if the accreted matter has solar composition. This is about three orders of magnitude lower than the average accretion rate of $\approx 10^{-16} M_\odot\,\mathrm{yr}^{-1}$ which is assumed by Dupuis et al. to account for the observed metal abundances. Therefore, the accretion of hydrogen must be effectively screened even onto these objects with high hydrogen abundances.

A detailed comparison of the observed abundances with the predictions of Dupuis et al. is not in the scope of this paper since the individual values depend on several free parameters. Such a comparison will be carried out in a future paper with a large set of homogeneously derived abundances.

Acknowledgements. We would like to thank the referee M. Barstow whose comments helped improving this paper. This work has been supported by the Deutsches Zentrum für Luft- und Raumfahrt (DLR) under grant 50 OR 96173. We have made use of the Simbad data base, operated at CDS, Strasbourg, France.

References

Allard N., Kielkopf J., 1982, Rev. Mod. Phys. 54, 1103
Allard N., Kielkopf J., 1991, A&A 242, 133
Allard N., Koester D., 1992, A&A 258, 464
Allard N.F., Koester D., Feautrier N., Spielfiedel A., 1994, A&AS 108, 417
Allard N.F., Drira I., Gerbaldi M., Kielkopf J., Spielfiedel A., 1998, A&A 335, 1124
Beauchamp A., Wesemael F., Bergeron P., 1997, ApJS 108, 559
Bergeron P., 1993, In: Barstow M.A. (ed.) White Dwarfs: Advances in Observation and Theory. Kluwer, Dordrecht, p. 267
Bergeron P., Wesemael F., Fontaine G., 1991, ApJ 367, 253

Bergeron P., Saumon D., Wesemael F., 1995, ApJ 443, 764
Bergeron P., Ruiz M.T., Leggett S.K., 1997, ApJS 108, 339
Chayer P., Fontaine G., Wesemael F., 1995, ApJS 99, 189
Däppen W., Mihalas D., Hummer D.G., Mihalas B.W., 1988, ApJ 332, 261
Dahn C.C., et al., 1987, Pub. US Naval Obs., Eighth Parallax List
Dupuis J., Fontaine G., Pelletier C., Wesemael F., 1992, ApJS 82, 505
Dupuis J., Fontaine G., Pelletier C., Wesemael F., 1993a, ApJS 84, 73
Dupuis J., Fontaine G., Wesemael F., 1993b, ApJS 87, 345
Finley D.S., Koester D., Basri G., 1997, ApJ 488, 375
Fontaine G., Graboske H.C.Jr., Van Horn H.M., 1977, ApJS 35, 293
Friedrich S., Koester D., Heber D., Jeffery C.S., Reimers D., 1999, A&A 350, 865
Hummer D.G., Mihalas D., 1988, ApJ 331, 794
Koester D., 1987. In: Davis Philip A.G., Hayes D.S., Liebert J.W. (eds.) The Second Conference on Faint Blue Stars, IAU Coll. No. 95, L. Davis Press, Schenectady, p. 329
Koester D., Allard N., 1995. In: Koester D., Werner K. (eds.) White Dwarfs. Springer, Berlin, p. 197
Koester D., Allard N.F., 1996. In: Jeffery C.S., Heber U. (eds.) Hydrogen-Deficient Stars. ASP Conf. Ser. Vol. 96, p. 224
Koester D., Weidemann V., Zeidler K.T.E.-M., 1982, A&A 116, 147
Kupka F., Piskunov N.E., Ryabchikova T.A., Stempels H.C., Weiss W.W., 1999, A&AS 138, 119
Kurucz R.L., 1991, In: Crivellari L., Hubeny I., Hummer D.G. (eds.) Stellar Atmospheres: Beyond Classical Methods. Kluwer, Dordrecht, p. 441
Lemke M., 1997, A&AS 122, 285
Liebert J., 1977, A&A 60, 101
Liebert J., Wehrse R., Green R.F., 1987, A&A 175, 173
Liebert J., Dahn C.C., Monet D.G., 1988, ApJ 332, 891
MacDonald J., Vennes S., 1991, ApJ 371, 719
Mihalas D., Däppen W., Hummer D.G., 1988, ApJ 331, 815
Mihalas D., Hummer D.G., Mihalas B.W., Däppen W., 1990, ApJ 350, 300
Nellis W.J., Holmes N.C., Mitchell A.C., et al., 1984, Phys. Rev. Lett. 53, 1248
Oke J.B., 1974, ApJS 27, 21
Pelletier C., Fontaine G., Wesemael F., Michaud G., Wegner G., 1986, ApJ 307, 242
Saumon D., Chabrier G., 1994, Phys. Rev. A 46, 2084
Saumon D., Chabrier G., Van Horn H.M., 1995, ApJS 99, 713
Schatzman E., 1949, Le Spectre des Naines blanches et leur Débit d'Énergie. Publikationer og mindre Meddelelser fra Københavns Observatorium Vol. 149, Copenhagen
Schatzman E., 1958, White Dwarfs. North-Holland Publishing Company, Amsterdam
Shipman H., Barnhill M., Provencal J., et al., 1995, AJ 109, 1231
Stancil P.C., 1994, ApJ 430, 360
Stone R.P.S., Baldwin J.A., 1983, MNRAS 204, 347
Theodorakopoulos G., Petsalakis I.D., Nicolaides C.A., Buenker R.J., 1987, J. Phys. B 20, 2339
van Altena W.F., 1998, Yale Catalog of Stellar Parallaxes
Vauclair G., Vauclair S., Greenstein J.L., 1979, A&A 80, 79
Vidal C.R., Cooper J., Smith E.W., 1973, ApJS 25, 37
Wesemael F., Truran J.W., 1982, ApJ 260, 807
Wolff B., Koester D., Dreizler S., Haas S., 1998, A&A 329, 1045
Wood M.A., 1994. In: Chabrier G., Schatzman E. (eds.) The Equation of State in Astrophysics. IAU Coll. 147, Cambridge University Press, p. 612
Zeidler K.T.E.-M., Weidemann V., Koester D., 1986, A&A 155, 356